HHS Public Access

Author manuscript

Nat Neurosci. Author manuscript; available in PMC 2014 February 01.

Published in final edited form as:

Nat Neurosci. 2013 August ; 16(8): 1049–1059. doi:10.1038/nn.3461.

Bidirectional NMDA receptor plasticity controls CA3 output and heterosynaptic metaplasticity

David L. Hunt[1], **Nagore Puente**[2], **Pedro Grandes**[2], and **Pablo E. Castillo**[1,*]

[1]Dominick P. Purpura Department of Neuroscience, Albert Einstein College of Medicine, Bronx, NY 10461

[2]Department of Neurosciences, Faculty of Medicine and Dentistry, University of the Basque Country UPV/EHU, E–48940 Leioa, Spain.

Abstract

N–methyl–d–aspartate glutamate receptors (NMDARs) are classically known as coincidence detectors for the induction of long–term synaptic plasticity, and have been implicated in hippocampal CA3–dependent spatial memory functions that likely rely on dynamic cellular ensemble encoding of space. The unique functional properties of both NMDARs and mossy fiber (MF) projections to CA3 pyramidal cells place MF–NMDARs in a prime position to influence CA3 ensemble dynamics. By mimicking pre and postsynaptic activity patterns observed *in–vivo*, we report a burst timing–dependent paradigm for bidirectional long–term NMDAR plasticity at MF–CA3 synapses in rat hippocampal slices. This form of plasticity imparts bimodal control of MF–driven CA3 burst–firing and spike temporal fidelity. Moreover, we show that MF–NMDARs mediate heterosynaptic metaplasticity between MF and associational/commissural synapses. Thus, bidirectional NMDAR plasticity at MF–CA3 synapses could significantly contribute to the formation, storage, and recall of CA3 cell assembly patterns.

Keywords

Burst–firing; mossy fiber; mGluR1; mGluR5; calcium; synapse; synaptic plasticity; STDP; LTP; LTD; hippocampus; learning; memory

Dynamic changes in synaptic strength are essential to neural information processing and likely underlie most forms of learning and memory. It is increasingly recognized that neural adaptations rely on a wide range of mechanistically different forms of activity–dependent synaptic plasticity, including, but not limited to, long–term potentiation (LTP) and depression (LTD) of excitatory transmission. At most excitatory synapses, α–amino–3–

*To whom correspondence should be addressed: Department of Neuroscience Albert Einstein College of Medicine 1410 Pelham Parkway South, Kennedy Center, Room 703 Bronx, NY10461 pablo.castillo@einstein.yu.edu.

Author Contributions D.L.H and P.E.C conceived the experimental design of the study. D.L.H performed and analyzed all electrophysiological experiments. N.P and P.G provided EM data and analysis. D.L.H and P.E.C interpreted the results and wrote the paper. All authors commented on the final version of the manuscript.

Competing Financial Interests The authors declare no competing financial interests.

hydroxy–5–methyl–4–isoxazolepropionic acid receptors (AMPARs) support fast transmission, whereas N–methyl–D–aspartate receptors (NMDARs) act as coincidence detectors –i.e., coincidence of glutamate release and postsynaptic depolarization– for the induction of long–term plasticity expressed as changes in AMPAR–mediated transmission. In addition to this classical role as coincidence detectors, NMDARs themselves can also mediate synaptic transmission and participate in long–term synaptic plasticity[1,2]. While NMDAR–LTP and NMDAR–LTD have been identified in several brain areas[2], when compared to AMPAR–mediated plasticity, NMDAR plasticity has been less well characterized. Furthermore, the precise contribution of NMDAR plasticity to information transfer at central synapses remains largely unexplored.

Due to the unique channel properties of NMDARs[3], dynamic regulation of these receptors can impact the flow of information and formation of cell assemblies[1,2]. Most NMDARs are blocked by Mg^{2+} at strong negative membrane potentials. However, the region of negative slope conductance from approximately −70 to −35 mV, leads to amplification of NMDAR–mediated currents during depolarization[4]. In addition, the slow kinetics of NMDAR–EPSPs, which allows for strong temporal summation, can produce a sustained level of excitation, thereby driving neuronal firing upon repetitive synaptic activity[5]. Recent studies have identified robust NMDAR–LTP at the mossy fiber (the axon arising from dentate granule cells or DGCs) to CA3 pyramidal cell synapse (MF–CA3)[6,7], a key excitatory input to the hippocampus. Induction of this form of LTP requires NMDAR and group 5 metabotropic glutamate receptor (mGluR5) co–activation, a postsynaptic Ca^{2+} rise and PKC activity. Unlike classical presynaptic LTP at MF–CA3 synapses[8], expression of MF–CA3 NMDAR–LTP is postsynaptic and likely due to NMDAR delivery to the synapse[6,7]. Compared to other hippocampal excitatory synapses, NMDAR–mediated synaptic responses are weak when elicited with single stimulations[9]. In fact, this modest contribution supports the classical view that MF–CA3 synapses do not express NMDAR–dependent forms of plasticity[8] (but see[10,11]), and raises questions about the actual role of NMDARs at these synapses. MF–CA3 synapses are well known for expressing uniquely robust frequency facilitation[8] and for their ability to fire the postsynaptic CA3 neuron, in particular during repetitive activity[12]. Both the NMDAR–EPSP slow kinetics and the burst–firing pattern of DGCs *in vivo*, make NMDARs at MF–CA3 synapses ideally suited to drive CA3 pyramidal neurons and shifts in the CA3 autoassociative network[13]. However, the precise contribution of NMDARs to DGC–CA3 spike transfer and whether NMDAR plasticity could participate in regulating this transfer under physiological conditions remains unknown.

In this study, we have investigated whether *in vivo*–like patterns of DGC and CA3 pyramidal cell activity[12,14] could elicit bidirectional NMDAR plasticity at MF–CA3 synapses. To this end, we have adapted the spatially selective burst–firing patterns of place cells to the paradigm of spike timing–dependent plasticity (STDP). Our results demonstrate that the temporal relationship between pre and postsynaptic bursting activity can dictate the polarity (LTP or LTD) and magnitude of NMDAR–mediated transmission. We further report that bidirectional NMDAR plasticity can modulate MF–driven burst–firing output and mediate heterosynaptic metaplasticity between MF synapses and associational/commissural (AC) synapses established between CA3 pyramidal cells. These forms of plasticity could

contribute to the formation, storage, and recall of cell assembly patterns in the hippocampal CA3 subfield.

RESULTS

Bidirectional, burst–timing dependent NMDAR plasticity at mossy fiber synapses

To investigate whether MF–CA3 synapses could undergo bidirectional NMDAR plasticity (i.e. LTP/LTD of the NMDAR–mediated component of MF synaptic transmission), we utilized burst–firing patterns of presynaptic DGCs and postsynaptic CA3 pyramidal neurons known to occur *in–vivo*[14]. We pharmacologically isolated NMDAR–mediated transmission (see Methods and Supplementary Table 1) and elicited MF–CA3 NMDAR–EPSCs by activating MFs with paired–pulse stimulation (5 ms inter–stimulus interval) while voltage–clamping CA3 pyramidal neurons at −50 mV. After a stable baseline (Supplementary Fig. 1), we paired presynaptic activity (5 stimuli, 50 Hz) with brief bursts of postsynaptic firing (3 action potentials, 100 Hz, elicited in current–clamp mode, V_m = −65 to −70mV, by 1 ms, 1.0–1.5 nA current injections; see Supplementary Table 2). These pairings were repeated 100 times at 2 Hz with various inter–burst intervals (timing interval). Positive timing intervals were measured from the last stimulation of the presynaptic burst and the first depolarization of the postsynaptic burst, whereas negative timing intervals were measured from the last depolarization of the postsynaptic burst and the first stimulation of the presynaptic burst. We found that a pre–post tetanus (+10 ms inter–burst timing interval) triggered a long–lasting enhancement of NMDAR–EPSCs ($tLTP_N$, 157 ± 8.1% of baseline, n = 10, p = 0.0078; Fig. 1a, c). Conversely, a post–pre tetanus (−10 ms inter–burst timing interval) lead to a depression of NMDAR–EPSCs ($tLTD_N$, 74 ± 3.3% of baseline, n = 9, p = 0.0056; Fig. 1b, c). On average, no synaptic plasticity was elicited at the overlap region (Fig. 1d). Synaptic plasticity was quantified by analyzing changes in NMDAR–EPSC amplitude 20–30 min after delivering the induction protocol. Consistent with NMDAR plasticity described at other synapses, both $tLTP_N$ and $tLTD_N$ developed relatively slowly over time, relative to AMPAR LTP and LTD[2]. Similar results were obtained at 32°C (Supplementary Fig. 2), and with both Wistar rats (Fig. 1) and Long Evans rats (Supplementary Fig. 3). Neither the presynaptic nor postsynaptic components of the pairing–protocol alone induced long–term plasticity of NMDAR–EPSCs (Fig. 1e). To investigate the timing requirements of $tLTP_N$ and $tLTD_N$ induction, we systematically varied the interval between the pre and postsynaptic bursts, and found that a timing interval of 250 ms yielded little to no plasticity, while a timing interval of 100 ms only induced $tLTD_N$ regardless of the order of pre or postsynaptic activation (Fig. 1d). Thus, like other forms of timing–dependent plasticity[15], the polarity and magnitude of NMDAR $tLTP_N$ and $tLTD_N$ are sensitive to the temporal relationship of pre and postsynaptic activity over a narrow time window.

In addition to NMDARs, glutamatergic transmission at MF–CA3 synapses is also mediated by AMPARs and kainate receptors (KARs). We therefore tested whether the induction protocols that trigger robust plasticity of NMDAR–EPSCs (Pre–post and Post–pre tetani, ± 10 ms timing interval) could also trigger long–term plasticity of AMPAR– and KAR–mediated transmission (see methods). However, neither of these protocols induced plasticity of AMPAR– or KAR–EPSCs (Fig. 1f,g)., Moreover, $tLTP_N$ and $tLTD_N$ were not associated

with changes in paired–pulse facilitation (PPF) or coefficient of variation (measured as $1/CV^2$) (Supplementary Fig. 4). Taken together, these findings indicate that both $tLTP_N$ and $tLTD_N$ are likely expressed postsynaptically as a selective change in NMDAR–mediated transmission rather than as a long–lasting change in glutamate release.

A role for Group–I metabotropic glutamate receptors in bidirectional NMDAR plasticity

Previous studies have shown that activation of group–I metabotropic glutamate receptors (mGluRs) is required for the induction of long–term plasticity of NMDAR–mediated transmission at central synapses[2]. While both mGluR1 and mGluR5 have been found at MF–CA3 synapses[16], only mGluR5 is required for NMDAR–LTP induced by repetitive stimulation of MFs[6,7]. To determine the role of group–I mGluRs in $tLTP_N$ and $tLTD_N$, we delivered our burst–pairing protocols (±10 ms timing intervals) in the presence of the specific mGluR5 and mGluR1 antagonists MPEP and LY367385 or CPCCOet, respectively. We found that 4 μM MPEP blocked $tLTP_N$ and partially suppressed $tLTD_N$, whereas 50 μM LY367385 or CPCCOet abolished $tLTD_N$ but had no effect on $tLTP_N$ (Fig. 2). These findings strongly suggest that mGluR5 and mGluR1 differentially regulate NMDAR plasticity at the MF–CA3 synapse. While mGluR5 plays an essential role for $tLTP_N$, mGluR1 is essential for $tLTD_N$.

We next tested the possibility that different topology of mGluR5 and mGluR1 could contribute to the selective role of these receptors in $tLTP_N$ and $tLTD_N$. To this end, we employed double postembedding immuno–electron microscopy for mGluR5/1b and performed quantitative measurements from the same sections (see Methods). We found that both mGluR5/1b co–localize within postsynaptic thorny excrescences in a relatively high proportion (≈38% of analyzed dendritic thorns, Fig. 3a–c). Consistent with previous observations[16], the majority (>60%) of gold particles for mGluR5/1b were found within 180 nm from the edge of the postsynaptic density (PSD). However, no topological differences in the subcellular localization between these receptors could be observed (Fig. 3d). In all, our functional and anatomical findings suggest that glutamate released during burst–firing stimulation similarly target mGluR1/5. It is therefore likely that some additional, context–dependent mechanism (see below) contributes to the selective role of these receptors in mediating the bidirectionality of burst timing–dependent NMDAR plasticity at MF–CA3 synapses.

Induction of bidirectional NMDAR plasticity relies on different calcium sources

To further investigate the mechanisms of $tLTP_N$ and $tLTD_N$ we next tested whether a rise in postsynaptic Ca^{2+} contributed to their induction (Fig. 4). We found that intracellular loading of the Ca^{2+} chelating agent BAPTA (20 mM) abolished both $tLTP_N$ and $tLTD_N$ ($tLTP_N$: 107.8 ± 4.2 % of baseline, n = 6, p = 0.0082; $tLTD_N$: 121 ± 18 % of baseline, n = 6, p = 0.0023, compared to interleaved controls, unpaired t–tests; Fig. 4h), indicating that postsynaptic Ca^{2+} rise is necessary for these forms of plasticity. The requirement for both mGluR5 activation and a postsynaptic Ca^{2+} rise in $tLTP_N$ induction resembles synaptically–induced MF–CA3 NMDAR–LTP[6,7]. To our knowledge, no previous studies have described LTD of NMDAR–mediated transmission at MF–CA3 synapses and therefore, we focused primarily on the further characterization of the underlying mechanism of $tLTD_N$. Several

Ca^{2+} sources could contribute to $tLTD_N$ induction, including Ca^{2+} influx via NMDARs, voltage–gated Ca^{2+} channels (VGCCs), and Ca^{2+} release from internal stores. To assess the role of NMDARs in the induction of $tLTD_N$, we bath applied the NMDAR antagonist d–APV transiently (25 μM, 5 min) during the POST–PRE induction protocol. Upon d–APV washout, no $tLTD_N$ was observed and NMDAR–mediated transmission was restored to baseline levels (control $tLTD_N$ in interleaved slices *vs*. d–APV during induction, p = 0.009, Fig. 4a,h), indicating that activation of NMDARs is necessary for $tLTD_N$ induction. The requirement of postsynaptic spiking activity for the induction of NMDAR plasticity (Fig. 1c,e), suggests that L–type VGCCs could contribute to a postsynaptic Ca^{2+} rise. Consistent with this prediction, we found that $tLTD_N$ was abolished in the presence of the L–type VGCC antagonist nifedipine (10 μM; p = 0.007 relative to interleaved controls, unpaired t–test, Fig. 4b,h). To investigate the contribution of Ca^{2+} from internal stores in MF–CA3 NMDAR plasticity, we depleted stores by incubating the slices in cyclopiazonic acid (CPA 30 μM for at least 30 min), which was also perfused throughout the recordings. Interestingly, CPA–treated slices failed to block the induction of $tLTD_N$ (p = 0.19 relative to interleaved controls, unpaired t–test, Fig. 4c,h), yet abolished $tLTP_N$ (p = 0.0021 relative to interleaved controls, unpaired t–test; Fig. 4d,h). This effect was also observed at more physiological temperatures (e.g. 32–35°C) (Supplementary Fig. 3). Together, these results not only indicate that multiple Ca^{2+} sources contribute to NMDAR plasticity, but also suggest that $tLTP_N$ and $tLTD_N$ have unique Ca^{2+} requirements for induction, with the PRE–POST, but not POST–PRE, induction protocol likely mobilizing enough Ca^{2+} from internal stores to induce plasticity.

$tLTD_N$ expression requires phosphatase and dynamin activity

We next examined the molecular basis of $tLTD_N$ expression. Previous studies at the Schaffer collateral to CA1 pyramidal cell synapse (Sch–CA1) have reported a form of synaptically–induced NMDAR–LTD that is likely due to lateral diffusion of NMDARs away from synaptic sites, a process resulting from destabilization of the cytoskeletal framework[17,18], and also requiring protein phosphatase 1 activity (PP1/2A)[17]. A similar form of Sch–CA1 NMDAR–LTD can be triggered by the group–I mGluR agonist DHPG, but this chemical form of plasticity does not seem to require phosphatase activity[19]. To test the role of PP1/2A in $tLTD_N$ at MF–CA3 synapses, we loaded the phosphatase inhibitor okadaic acid (1 μM) into CA3 pyramidal cells via the patch pipette. Like synaptically–induced NMDAR–LTD at Sch–CA1 synapses, this manipulation completely blocked $tLTD_N$ at MF–CA3 synapses (p = 0.0042 relative to interleaved controls; Fig. 4e,h). However, unlike Sch–CA1 synapses, intracellular loading of both GDP–βS (600 μM), which impairs all GTP–dependent activity (including that of dynamin and mGluR1/5), and the dynamin inhibitory peptide (DIP, 50 μM), which specifically interferes with dynamin–dependent endocytosis, blocked $tLTD_N$ (GDP–βS: p = 0.011 relative to interleaved controls, Fig. 4f,h; DIP: p = 0.0073 relative to interleaved controls; Fig. 4g,h). Overall, our results indicate that $tLTD_N$ at MF–CA3 synapses is likely due to internalization of postsynaptic NMDARs via dynamin–dependent endocytosis.

Bidirectional plasticity of mossy fiber–driven burst firing output

Although NMDAR function has been traditionally associated with the induction of AMPAR–mediated LTP and LTD, postsynaptic NMDARs can also support other functions, including burst–firing[1,2,5]. To directly address this possibility at the MF–CA3 synapse, we monitored MF–induced action potentials (APs) in CA3 pyramidal cells in current–clamp mode under normal recording conditions (i.e., no drugs included in the bath), and delivered brief bursts of suprathreshold MF stimulation (5 stimuli, 50 Hz, repeated every 30 s; see Supplementary Table 2) that typically elicited 2–3 spikes/burst. After a stable baseline, NMDAR–mediated transmission was selectively blocked by the use–dependent, non–competitive NMDAR channel blocker MK–801. We found that bath application of 50 μM MK–801 significantly reduced the number of CA3 APs/burst compared to naïve interleaved slices (MK–801: 64 ± 6.2 % of baseline, n = 6; p = 0.0062; Supplementary Fig. 5). Thus, NMDAR transmission at MF–CA3 synapses can drive CA3 pyramidal cells during presynaptic burst activity patterns.

We next sought to determine whether induction of $tLTP_N$ and $tLTD_N$, by strengthening or weakening NMDAR transmission, could impact MF–driven spiking output of CA3 pyramidal cells. To this end, we elicited APs from CA3 pyramidal neurons in the absence of drugs as above, but in this case MF stimulation was gauged to trigger 1–2 APs/burst on average for each presynaptic stimulation. After monitoring a stable baseline, the pre–post ($tLTP_N$) protocol induced a robust long–lasting enhancement in the number of spikes/burst (Fig. 5a–c, 168 ± 20 % of baseline, n = 8, p = 0.0014). Importantly, and similar to $tLTP_N$ (Fig. 2a), this enhancement was abolished in the continuous presence of 4 μM MPEP (Fig. 5b,c). To assess whether induction of $tLTD_N$ could affect MF–driven spiking output of CA3 pyramidal cells, baseline stimulation was set to elicit 2–4 APs/burst. Under these conditions, the post–pre ($tLTD_N$) protocol induced a long–lasting decrease in the resulting spikes/burst (Fig. 5d–f; 29 ± 7.8 % of baseline, n = 7, p = 0.004), and this reduction was impaired in the presence of 50 μM LY367385 (Fig. 5e,f), consistent with the effect of mGluR1 antagonism on $tLTD_N$ (Fig. 2b). None of these burst–induced shifts in spiking output were associated with changes in input resistance (R_i) (Fig. 5b,e). Absolute values of spikes/burst showed that the baseline values for control and block experiments were comparable within the pre–post and post–pre protocols (Fig 5c,f). None of the antagonists, MPEP and LY367385, had any significant effect on basal synaptic transmission (Supplementary Fig. 6). Finally, we measured the mean spike latency and coefficient of variation of spike latency values (jitter) before and after burst plasticity, and found that these forms of plasticity were accompanied by bidirectional changes in spike temporal fidelity. Indeed, induction of $tLTP_N$ resulted in shorter spike latencies and reduced jitter (Fig. 6a–c), whereas induction of $tLTD_N$ led to longer spike latencies and increased jitter (Fig. 6d–f). Collectively, these findings show that bidirectional NMDAR plasticity at MF–CA3 synapses can modulate spike transfer and temporal fidelity of MF–driven output of CA3 pyramidal cells.

Heterosynaptic metaplasticity mediated by mossy fiber NMDARs

Metaplasticity, the plasticity of synaptic plasticity, generally refers to a shift in the inducibility of synaptic plasticity[20]. Given their role as triggers of long–term plasticity, changes in NMDAR function or number are expected to shift the induction threshold for

NMDAR–dependent forms of LTP and LTD. At the MF–CA3 synapse, a recent study has reported NMDAR–dependent homosynaptic metaplasticity of AMPAR–mediated transmission[10]. Whether NMDAR plasticity at MF synapses could play a role in heterosynaptic metaplasticity (i.e. plasticity at neighboring AC synapses) is unknown. Previous work indicated that the temporal overlap of activated MF and AC synapses at CA3 pyramidal neurons can facilitate potentiation of AC synapses, an effect that could be mediated, at least in part, by an as–yet–unidentified, slow–acting factor provided by MF stimulation[21].

To test whether MF–NMDARs could participate in this form of heterosynaptic metaplasticity between MF and AC synapses, we first evaluated the impact of blocking NMDAR–mediated transmission at MF–CA3 synapses. To this end, we took advantage of the NMDAR activity–dependent blocker MK–801 and carried out a two–pathway experiment, whereby we monitored AC and MF–evoked EPSPs from the same CA3 pyramidal cell (Fig. 7). These experiments were also performed under normal recording conditions (i.e., no drugs included in the bath). Two experimental conditions were employed, one in which MF stimulation was sustained throughout a 10 min MK–801 wash–in period, and the other where MF stimulation was stopped during wash–in. AC stimulation was stopped for both experimental conditions. This strategy largely spared AC–NMDARs from MK–801 blockade during MF stimulation, enabling induction of NMDAR–dependent AC–LTP, while selectively blocking (*MF–on*), or not blocking (*MF–off*) MF–NMDARs. Following MK–801 application, stimulation was resumed for both pathways. A tetanus consisting of 10 paired bursts (5 pulses, 100 Hz, delivered at 5 Hz)[21] was then applied simultaneously to the MF and AC pathways, calibrated such that each pathway alone was subthreshold for AP firing, but together became suprathreshold, followed by an additional 5 unpaired bursts of AC stimulation (Fig. 7a; Supplementary Table 2). This induction paradigm is designed to capture the essential activity–dependent requirements for heterosynaptic plasticity, namely, high temporal overlap between MF and AC stimulation, and late unpaired AC stimulation to capitalize on a putative slow–acting factor that facilitates the heterosynaptic interaction[21]. In all experiments, the MF + AC stimulation protocol was delivered less than 20 min after break–in, to avoid wash–out of AC LTP. We observed that when MF stimulation is sustained during MK–801 wash–in (*MF–on*), AC–LTP is attenuated relative to non–stimulated controls (Fig. 7b–d). The magnitude of MK–801 blockade of MF–CA3 NMDAR transmission during the 10 min wash–in period was measured in a separate set of experiments by pharmacologically isolating NMDAR–EPSPs, where we saw 52 ± 8% blockade of NMDAR transmission (Fig. 7e). Subthreshold stimulation of either MF or AC inputs alone did not reliably lead to spiking. However, coincident MF + AC stimulation yielded spiking output, which was comparable when MF–NMDARs were partially blocked or unblocked (*MF–on*; 14.5 ± 2.2 spikes, n = 10, *MF–off* 14.8 ± 1.5 spikes, n = 10, p = 0.1762; Supplementary Figure 7a). Likewise, baseline EPSP amplitudes were comparable under control and partial block of MF NMDAR conditions (Supplementary Figure 7b). These observations strongly suggest that the difference in AC plasticity could not be explained by firing alone or differences in baseline synaptic transmission. Our results not only support the notion that MF–NMDARs can heterosynaptically contribute to the induction of plasticity at AC synapses, but also suggest

that NMDAR–LTD at MF–CA3 synapses, here mimicked by pharmacological blockade with MK–801, could impart heterosynaptic metaplastic control over AC synapses.

To more rigorously test the hypothesis that MF–NMDARs and NMDAR plasticity enables heterosynaptic metaplasticity, we employed a synaptic induction protocol. While previous experiments utilized current injections to elicit the temporally precise APs necessary for NMDAR plasticity (Figs. 1–2, 4–5), presynaptically driven spikes are more physiological and closely mimic our PRE–POST induction paradigm. We therefore monitored NMDAR–EPSPs (see Methods and Supplementary Table 1) and used a suprathreshold tetanus of 5 presynaptic pulses at 50 Hz, delivered 50 times at 5 Hz (theta frequency) (Fig. 8a). This protocol induced robust MF–CA3 NMDAR LTP, a phenomenon that we called LTP_N. Presumably, LTP_N is mechanistically similar to tLTPN as it is blocked by 4 μM MPEP (Fig. 8b). Like for $tLTP_N$ (Fig. 1g), the LTP_N induction protocol did not trigger LTP of KAR–EPSPs (Supplementary Fig. 8). Under normal recording conditions (no drugs in the bath), the LTP_N tetanus selectively potentiated the slow excitatory component of mixed MF responses, which is largely blocked by 50 μM d–APV; Supplementary Fig. 8), while basically sparing the fast, AMPAR–mediated component (Fig. 8c). Moreover, mGluR5 blockade with MPEP abolished LTP_N but had no effect on AMPAR–mediated transmission (Fig. 8d). These findings strongly suggest that presynaptically driven spiking by theta–patterned MF bursting activity can also selectively potentiate NMDAR–mediated transmission under normal recording conditions.

To test whether LTP_N can trigger heterosynaptic metaplasticity at AC synapses we conducted a 2–pathway experiment in which the LTP_N was delivered in the cell–attached configuration (to avoid LTP washout) in the presence or absence of 4 μM MPEP, to block or spare the induction of LTP_N, respectively. MPEP was immediately washed–out following LTP_N induction tetanus, and 10 min later we switched to the whole–cell recording configuration (break–in) and began baseline acquisition. After a 10 min baseline, when LTP_N is robust (20 min post–tetanus), we delivered the MF + AC pairing induction protocol (Fig. 7a). We observed that AC–LTP is enhanced relative to MPEP treated slices (Fig. 8e). MPEP did not significantly affect the spiking output of CA3 pyramidal cells in any of our experimental conditions ($p \geq 0.09$; Supplementary Fig. 7c). Given that long–lasting decreases in inhibitory synaptic transmission can mediate metaplasticity[20], changes in inhibition could have contributed to heterosynaptic plasticity in CA3 neurons. However, neither the inhibitory component of the complex response evoked under normal conditions (i.e. no drugs in the bath), nor IPSCs monitored at 0 mV, showed any evidence of inhibitory synaptic depression following the induction of NMDAR plasticity (Supplementary Fig. 10). It is therefore unlikely that heterosynaptic metaplasticity could be due to disinhibition. Consistent with a depolarization–independent factor as a principal contributor to the heterosynaptic induction of AC–LTP[21], we found no positive correlation between APs during LTP_Ntet and the subsequent induction of LTP_N or AC–LTP (Supplementary Figure 7d). In this context, it is worth noting that the MF AMPAR–mediated component remained slightly potentiated post–LTP_Ntet, at the time the MF+AC protocol was delivered (Fig. 8c), raising the possibility that this component could have contributed to heterosynaptic metaplasticity. However, against this scenario are the following observations. The absolute value of AC–LTP achieved in MPEP(+) trials (Fig. 8e) and in the MF–off trials (Fig. 7d)

was not significantly different (p = 0.14; Supplementary Figure 7e). These two conditions can be considered analogous in that in both cases MF NMDAR–mediated transmission has not been modified in either direction. If MF AMPAR–mediated transmission played any significant role in heterosynaptic induction of AC–LTP, then one would expect more plasticity in MPEP(+) trials than in MF–off trials, which is not the case. Moreover, MPEP interferes with heterosynaptic metaplasticity (Fig. 8e) without modifying AMPAR transmission (Fig. 8d). In conjunction with results presented in Fig. 7, our findings strongly support a role for MF–NMDARs and bidirectional NMDAR plasticity in the heterosynaptic metaplastic control of AC–LTP. In addition to MF–NMDAR dependent mechanisms of heterosynaptic plasticity, Ca^{2+} waves initiated at the MF synapse could actively propagate via IP_3 receptor (IP_3R)–mediated calcium release to more distal AC dendritic regions[22,23], thereby facilitating the induction of AC–LTP. To test the contribution of IP_3Rs in heterosynaptic plasticity, we loaded CA3 cells with heparin and delivered our MF + AC pairing protocol. We observed that AC–LTP was largely attenuated in heparin–loaded cells relative to interleaved controls while leaving the peak MF–EPSP and the number of spikes during the MF + AC pairing unaffected (Supplementary Figs. 7a,b and 11). These results suggest that, in addition to MF–NMDARs, IP_3Rs could contribute to heteroassociative plasticity between MF and AC synapses.

DISCUSSION

Here we report that patterns of bursting activity similar to those observed by DGCs and CA3 pyramidal neurons *in vivo* can trigger long–lasting strengthening ($tLTP_N$) or weakening ($tLTD_N$) of NMDAR–mediated transmission at the MF–CA3 synapse *in vitro*. Mechanistically, $tLTP_N$ resembles the recently identified MF–NMDAR LTP, which is normally triggered by presynaptic tetanic stimulation[9,10]. Induction of both $tLTP_N$ and synaptically–induced NMDAR LTP requires mGluR5/NMDAR co–activation and postsynaptic Ca^{2+} rise, including Ca^{2+} release from internal stores. In this study, we have also discovered and characterized $tLTD_N$, in which induction requires NMDAR/mGluR1 co–activation and Ca^{2+} influx via L–type Ca^{2+} channels, but not Ca^{2+} stores, and expression is likely due to dynamin–dependent endocytosis of NMDARs. We also report that NMDAR plasticity can bidirectionally control MF–driven burst–firing output and spike temporal fidelity of CA3 pyramidal neurons. Moreover, MF–NMDARs can exert metaplastic control of AC–LTP. These newly described functions of NMDARs at MF–CA3 synapses can enable regulation of CA3 ensemble dynamics and may play a significant role in CA3–dependent memory formation[24-26].

Burst timing–dependent NMDA receptor plasticity

In contrast to classical STDP protocols (that typically utilize single pulses, although more complex patterns have been tested[15]), we have adopted a burst timing–dependent paradigm to investigate the functional role and regulation of postsynaptic MF–NMDARs (Fig. 1a,b). The physiological relevance of this paradigm is several–fold. Bursts (brief epochs of high–frequency discharge) represent a stereotypical firing pattern exhibited by both DGCs and CA3 pyramidal cells *in vivo* during exploratory behaviors, place cell activation, active sleep and spatial memory formation[12,14,27]. Moreover, within the DG–CA3 microcircuit, the

excitation/inhibition ratio remains balanced at lower frequencies of MF activity[28]; however, short–term synaptic plasticity within this microcircuit (i.e., short–term depression of somatically projecting feed–forward inhibitory inputs, and short–term facilitation at MF–CA3 synapses) tilts the excitation/inhibition balance towards excitation at higher frequencies[29], where the influence of the NMDAR will be more pronounced[1,5]. This "frequency gating" property of the MF–CA3 synapse acts as a filter, selectively propagating bursting activity from the DG to CA3[12,30]. This attribute exemplifies the notion that bursts convey particularly salient inputs, and represent a unit of neural information[31]. As MF–NMDARs participate in MF–driven burst–firing of CA3 pyramidal cells, bidirectional NMDAR plasticity may play an important role in regulating the burst–mediated flow of information through the hippocampal tri–synaptic circuit during exploratory behaviors. Albeit induced with different stimulation protocols, burst timing–dependent LTP and LTD of NMDAR–mediated transmission has also been reported in midbrain dopamine neurons[32]. This observation, together with our findings, suggests that bidirectional, burst timing–dependent NMDAR plasticity could be a general phenomenon in the central nervous system. –

Analysis of the burst–timing requirements for induction of $tLTP_N$ and $tLTD_N$ revealed a Hebbian synaptic learning rule (Fig. 1d): the MF–CA3 synapse will increase its efficacy only when the presynaptic input arrives within a narrow time window before a postsynaptic response; otherwise efficacy decreases. The fact that $tLTD_N$ is equally triggered by ±100 ms (pre–post and post–pre) timing intervals suggests two distinct thresholds[33] for induction of $tLTP_N$ and $tLTD_N$, consistent with the notion that the polarity of plasticity is principally determined by the amplitude and/or time–course of postsynaptic Ca^{2+} rise[15,33,34]. Thus, this learning rule could arise if an initial indiscriminate Ca^{2+} threshold (similarly generated by 100 ms pre–post and post–pre timing intervals) led to $tLTD_N$, whereas $tLTP_N$ could then be induced only with additional Ca requirements (i.e., Ca^{2+} release from internal stores) achieved by shorter pre–post timing intervals (+10 ms). While this Ca^{2+}–dependent hypothesis of induction is consistent with other forms of STDP[33], future studies will be required to directly test the spatiotemporal Ca^{2+} dynamics of burst–timing dependent NMDAR plasticity.

Previous work has shown that mGluR1 and mGluR5 subtypes can have distinct physiological roles[35,36] and signal through diverse intracellular pathways[37], including at the MF–CA3 synapse[38]. The presence of these two receptors at the same postsynaptic thorns (Fig. 3) prompts the question of what roles these receptors play in synaptic transmission and plasticity. Most likely, these receptors are co–activated to a similar extent during our pre–post and post–pre induction protocols. Coincident occurrence of Ca^{2+} release from internal stores could suppress the mGluR1 signaling cascade normally leading to $tLTD_N$, allowing mGluR5 signaling to dominate, and $tLTP_N$ expression to occur. This "veto" effect[39] suggests a point (or points) of convergence between the signaling cascades downstream of receptor activation, where the activated mGluR5 pathway can antagonize the mGluR1 pathway contingent on an appropriate Ca^{2+} signal, such as Ca^{2+} release from internal stores. Support for this hypothesis comes from our analysis of the various Ca^{2+} sources required for induction of both $tLTP_N$ and $tLTD_N$, in that $tLTP_N$ requires Ca^{2+} from internal stores, NMDARs, and L–type Ca^{2+} channels. Together, our data suggest that the postsynaptic thorn

could integrate afferent activity via signaling pathways initiated by group–I mGluR activation, and the concomitant spatiotemporal Ca^{2+} dynamics generated by that afferent activity pattern. This notion is in agreement with a recent study suggesting that a particular pattern of intracellular Ca^{2+} transients (e.g. triggered by low–frequency pairing stimulation of MFs) could be critically involved in the induction of a mGluR1–dependent, but mGluR5–independent short–lasting potentiation of MF–CA3 synaptic transmission[38]. These observations, in conjunction with the present study, underscore how the precise timing and pattern of MF activation can engage mechanistically different forms of plasticity. While most studies, including ours, utilize bulk stimulation to activate MFs, it remains to be seen whether synaptic cooperativity is necessary, or whether activation of a single MF is sufficient to induce NMDAR plasticity. Finally, previous studies have reported that NMDAR LTD at Sch–CA1 synapses is due to lateral diffusion of NMDARs away from synaptic sites[17,18], a process requiring phosphatase activation[17]. Although similar phosphatase activation is required for $tLTD_N$, dynamin–dependent endocytosis seems to underlie this form of plasticity.

Functional significance of NMDA receptor plasticity

In the context of learning and memory, the storage and retrieval of a given neuronal ensemble pattern likely relies on synaptic plasticity between activated cells[27,40]. A potential mechanism meeting this requirement is described by coincident bursting activity between CA3 pyramidal cells, leading to the specific modification of AC synaptic weight[41]. The privileged nature of MF input in driving CA3 bursting output[12] places MF–NMDARs in an advantageous position to support the heterosynaptic interaction between MF and AC synapses by modulating the burst propensity of CA3 pyramidal cells[21]. In support of this scenario is the bidirectional modulation of CA3 burst–firing output (Fig. 5). Greater or lesser burst–firing output of CA3 pyramidal neurons would lead to stronger or weaker AC synaptic strength, promoting the formation or disbandment of recurrently connected CA3 ensembles respectively. Moreover, dysregulation of NMDAR plasticity at MF–CA3 synapses could play a role in pathological conditions of excitability where aberrant bursting activity may trigger epileptiform events.

In cortical microcircuits with somatically projecting feed–forward inhibition (such as the MF–CA3 connection[42]), the temporal fidelity of APs can rely on the time window with which EPSPs and IPSPs integrate to elicit APs[43]. However this mechanism does not appear to control temporal fidelity at the MF–CA3 synapse[28]. The observation that $tLTP_N$ and $tLTD_N$ can bidirectionally modulate spike temporal fidelity (jitter, Fig. 6) is likely relevant to the heterosynaptic control of STDP at AC inputs (AC–STDP)[44], given that millisecond range changes in the timing of pre– or postsynaptic activity can yield sizable changes in the resulting plasticity that is induced[15,33]. Increases in jitter would increase the probability that back–propagating spikes arrive at AC synaptic sites with longer latencies, leading to shifts in the polarity and/or magnitude of AC–STDP. Decreases in jitter would have the converse effect, sharpening the timing requirements for AC learning rules[45]. Thus, the impact of burst plasticity mediated by $tLTP_N$ and $tLTD_N$ can affect cellular ensemble coding in CA3 by parallel mechanisms, namely via controlling spiking output (Fig. 5) and temporal fidelity of APs (Fig. 6). Bidirectional modulation of CA3 burst–firing output could increase or

decrease the magnitude of AC plasticity during spatial memory formation, preferentially linking cells with greater burst–firing output[41]. The accompanying modulation of spike temporal fidelity could prove important by influencing AC–STDP learning rules, governing which cells are functionally incorporated or removed from a given cell assembly linked by recurrent synaptic strength.

In addition to the action potential–dependent mechanisms discussed above, heterosynaptic adjustment of AC synaptic weight by $tLTP_N$ and $tLTD_N$ may serve as an additional mechanism for tuning ensemble activity in CA3. Previous studies have reported that MF–NMDARs heterosynaptically adjust perforant path, but not AC synapses on CA3 cells[46], or homosynaptically act as a metaplastic switch required for AMPAR–mediated plasticity at the MF–CA3 synapse[10] (see also[11]). In contrast, we report that MF NMDARs (Fig. 7) and LTP_N at the MF–CA3 synapse (Fig. 8) can heterosynaptically modify induction of LTP at AC synapses. Of note, robust LTP_N at MF–CA3 (Fig. 8a,b) did not enable subsequent MF AMPAR LTP using an induction protocol that triggered AC AMPAR LTP (Fig. 8c). This observation suggests that MF–CA3 synapses might have a relatively high induction threshold for the induction of postsynaptically–expressed AMPAR LTP. Through modulation of AC synaptic strength MF–NMDARs could promote the incorporation and/or removal of individual cellular activity from the ensamble code by facilitating induction of synaptic plasticity at recurrent connections.

How could MF activation heterosynaptically facilitate the induction of AC AMPAR LTP? It has been proposed that MF activity likely provides a slow–acting factor that travels distally and targets AC synapses[21]. Intriguingly, pharmacological blockade of mGluR1 during MF + AC co–stimulation blocked associative AC LTP but the downstream signaling pathway remained unidentified[21]. Here we provide evidence that NMDARs at MF–CA3 synapses contribute to heterosynaptic metaplasticity of AC AMPAR LTP. While future studies will be required to address the detailed mechanism underlying this process, two parsimonious candidate mechanisms emerge. One possibility is direct heterosynaptic spread[47] of MF–NMDAR–mediated Ca^{2+} to AC dendritic regions, which can be enhanced by supralinear integration of NMDAR–EPSPs[4,48]. Alternatively, Ca^{2+} waves may be actively propagated along the dendritic endoplasmic reticulum[23]. In support of this scenario, Ca^{2+} from internal stores in CA1 pyramidal neurons can regulate the polarity and input–specificity of long–term synaptic plasticity[49], and also mediate heterosynaptic metaplasticity in an action potential–independent manner[50]. While these potential mechanisms are not necessarily mutually exclusive, the latter possibility is particularly appealing given that co–activation of NMDARs and mGluRs at MF–CA3 synapses are known to initiate intracellular Ca^{2+} waves that can propagate to more distal dendritic domains[22].

METHODS

Electrophysiology

Hippocampal slices were prepared from both male and female Wistar and Long Evans rats (17–30 days old; CharlesRiver). All animal procedures were carried out in accordance with the National Institutes of Health Guide for the Care and Use of Laboratory Animals. After animals were deeply anesthetized with isoflurane, they were decapitated and the brain

rapidly removed into chilled cutting solution consisting of (in mM) 215 sucrose, 2.5 KCl, 20 glucose, 26 $NaHCO_3$, 1.6 NaH_2PO_4, 1 $CaCl_2$, 4 $MgCl_2$, and 4 $MgSO_4$. Hippocampi were dissected out and cut into 400 μm thick transverse sections on a DTK–2000 vibrating microslicer (Dosaka EM Co., Ltd., Japan) or a VT1200s microsclicer (Leica Microsystems Co., Ltd., Germany). The cutting solution was slowly exchanged with artificial cerebrospinal fluid (ACSF) containing (in mM) 124 NaCl, 2.5 KCl, 10 glucose, 26 $NaHCO_3$, 1.0 NaH_2PO_4, 2.5 $CaCl_2$, and 1.3 $MgCl_2$. Both cutting and ACSF solutions were saturated with 95% O_2 and 5% CO_2 (pH 7.4). The slices were incubated at room temperature for at least 1.5 hr before recording. The slices were then transferred as needed to a submersion–type recording chamber and were perfused with ACSF (2 ml/min).

Whole–cell recordings of CA3 pyramidal cells were obtained using standard techniques. To maximize cell health and recording stability, cells deep below the surface of the slice were recorded “semi–blind”. The recording pipette resistance ranged between 3 and 4 MΩ. Series resistance (6–15 MΩ) and input resistance were monitored throughout each voltage–clamp recording with 80 ms, –4 mV steps. Recordings with >10% change in series or input resistance were systematically excluded. The pipette solution for all recordings contained (in mM) 135 K–gluconate, 5 KCl, 1 $CaCl_2$, 0.1 EGTA, 10 HEPES, 10 glucose, 5 MgATP, and 0.4 Na_3GTP. In current clamp mode, this internal solution (8 mV liquid junction potential, uncorrected) yielded a resting membrane potential that ranged from –69 to –58 mV. Maximal recording time after dissection was 6 hr. To maximize stability during long–term whole–cell recording as well as cell health, experiments were performed at 25.0°C ± 0.1°C (unless stated differently) using a TC–344B dual–channel temperature controller (Warner Instruments, Inc, Hamden, CT, USA).

Synaptic afferents were activated by monopolar stimulation delivered via a patch–type pipette broken to a tip diameter of ≈10 μm and filled with ACSF. This stimulating electrode was placed in the dentate gyrus cell body layer to activate MFs and in the CA3 *s. radiatum* (100–150 μm apical to *s. lucidum*) to activate AC fibers. All stimulation protocols are summarized in Supplementary Table 2. The baseline stimulation rate was 0.1 Hz for all experiments. To elicit baseline responses of 50–100 pA or 5–10 mV on average, 100–500 μA stimulation pulses of 100–200 μs duration were used. To confirm that the activated afferents were not significantly contaminated by AC inputs, 1 μM DCG–IV, a group II mGluR agonist that blocks MF but not AC synaptic transmission, was applied at the end of every experiment, and the data were accepted only if synaptic responses were reduced by more than 80%. The synaptic response remaining in DCG–IV was then subtracted from all previous responses before further analysis to isolate MF–specific synaptic activity. Unless otherwise noted, NMDAR–EPSCs were elicited by paired–pulse stimulation (5 ms or 40 ms inter–stimulus interval, ISI) in the presence of 10 μM NBQX, 100 μM picrotoxin, and 3 μM CGP55845, to block AMPA/KA, $GABA_A$ and $GABA_B$ receptors, respectively, while voltage–clamping to –50 mV. For KAR–EPSCs, the selective AMPAR antagonist GYKI53655 (30 μM) was used and cells were voltage–clamped to –70 mV. The identity of KAR–EPSCs was confirmed by the addition of 10 μM NBQX at the end of each experiment. KAR–mediated MF–CA3 EPSCs were evoked by single stimulation in the dentate gyrus. AMPAR–EPSCs were elicited using single–pulse stimulation, recorded in the absence of

drugs in the bath while voltage clamping at –70 mV (i.e., at $GABA_AR$ reversal), and included in the analysis based on their characteristically fast kinetics (~1 ms rise time). The various pharmacological contitions used in this study are summarized in Supplementary Table 1.

All experiments were executed with a MultiClamp 700B (Axon Instruments/Molecular Devices, Union City, CA, USA). Electrophysiological data were filtered (2.5 KHz), digitized (3–5 KHz), and analyzed using custom–made software for IgorPro (Wavemetrics Inc., Lake Oswego, OR, USA). NBQX, D–APV, picrotoxin, CGP55845, DCG–IV, GYKI53655, MPEP, LY367385, CPCCOet, dynamin inhibitory peptide, Nifedipine, okidaic acid, MK–801, and cyclopiazonic acid were obtained from Tocris–Cookson Inc. (Ellisville, MO, USA). BAPTA, and all other chemicals were purchased from Sigma–Aldrich (St. Louis, MO, USA), and GDP–βS was purchased from Biomol (Plymouth Meeting, PA, USA).

Postembedding Immunogold Electron Microscopy

Tissue preparation—To preserve ultrastructure optimally, 3 rats were first anesthetized and perfused through the heart with a fixative solution containing 0.1% glutaraldehyde and 4% depolymerized paraformaldehyde, prepared in 0.1 M PB (pH 7.4). Small rectangular pieces measuring 0.5 × 0.5 × 1 mm from the hippocampus CA3 region were rinsed in PB (4°C, overnight), cryoprotected in glycerol (10%, 20%, and 30% in PB), and rapidly frozen in liquid propane in a cryofixation unit (KF80; Reichert, Vienna, Austria). They were then freeze–substituted with methanol and 0.5% uranyl acetate, and subsequently embedded in Lowicryl HM20 (Lowi, Waldkraiburg, Germany).

Immunocytochemistry—Ultrathin sections (70 nm) were collected on nickel grids coated with an adhesive film (Formvar). They were then washed in Tris–buffered saline with Triton X–100 (TBST: 50 mM Tris–HCl, pH 7.4; 0.15 M NaCl; 0.1% Triton X–100; 0.02% NaN_3) containing 0.1% $NaBH_4$ and 50 mM glycine for 10 min, and rinsed 3 times for 1 min in TBST. Tissue sections were preincubated in blocking solution: 10% (w/v) bovine serum albumin (BSA) in TBST for at least 10 min. Then, they were incubated overnight with a mixture of affinity–purified primary mGluR1b (2 μg/ml) and mGluR5 (20 μg/ml) antisera in TBST with 2% BSA. The polyclonal mGluR1b antibodies were raised in rabbit against the carboxy–terminal amino acid sequence of the rat mGluR1b (amino acid residues 887–906). The polyclonal mGluR5 antibodies were raised in guinea pig against the carboxy–terminal amino acid sequence of the mouse mGluR5 (amino acid residues 1144–1171; Frontier Institute Co. Ltd; 1–777–12, Shinko–nishi, Ishikari, Hokkaido, Japan; code number: mGluR5–GP–Af270–1). Both antibodies were extensively characterized and the characteristic labeling in wildtype tissue disappeared in the brains of mGluR1 and mGluR5 knock–out mice[51-54]. Tissue processing was followed by thorough washes in TBST, preincubated with the blocking solution for 10 min, and then incubated with a mixture of secondary antibodies coupled to different sizes of colloidal gold particles: goat F(ab')2 anti–rabbit IgG fragments coupled to 10–nm colloidal gold particles for mGluR1b (GFAR10; British Biocell International, Cardiff, UK) and goat anti–guinea pig IgG fragments coupled to 20–nm colloidal gold particles for mGluR5 (GAG20; British Biocell International,

Cardiff, UK) diluted 1:20 in TBST containing 2% BSA. Finally, the grids were rinsed several times in double–distilled water, counterstained with uranyl acetate and lead citrate, and examined in a PHILIPS EM2008S electron microscope. Tissue preparations were photographed by using a digital camera coupled to the electron microscope. Figure compositions were scanned at 500 dots per inch (dpi). Labeling and minor adjustments in contrast and brightness were made using Adobe Photoshop (CS, Adobe Systems, San Jose, CA, USA).

Data analysis and statistics

Electrophysiology—The magnitude of plasticity was always assessed relative to interleaved controls and was quantified by averaging synaptic responses, for 10 min periods right before and 20–30 min after the induction protocol (unless otherwise stated). Statistical significance between means was calculated using two–sided Student's t test using OriginPro software. Paired t–test was used to compare baseline with responses post–induction, whereas unpaired t–test was used to compare experimental manipulations with interleaved control experiments. In all figures, error bars indicate ± SEM, and averaged traces include 15–30 consecutive individual responses. In order to better visualize the shifts in spike latency before and after plasticity (Fig. 6d,e), spike latency distributions were fitted with a Lorentz curve using OriginPro software. In all cases "n" refers to a single cell experiment from single slice. While we did not track the number of animals used we estimate that overall 100 animals from 50 litters were utilized. No statistical methods were used to pre–determine sample sizes. Data collection and analysis were not performed blind to the conditions of the experiment.

Electron microscopy—A total of 247 thorny excrescences of pyramidal neurons receiving typical mossy fiber synapses in CA3 *stratum lucidum* (total area studied: 811.86 μm^2) were measured and analyzed by NIH Image–J (version 1.36; National Institute of Mental Health, Research Services Branch, National Institutes of Health, Bethesda, MD, USA). The percentage of the dendritic thorns immunopositive and immunonegative for mGluR1b and/or for mGluR5, was analyzed and displayed using a statistical software package (GraphPad Prism 4, GraphPad Software Inc, San Diego, CA, USA). Positive labeling was considered if at least one gold particle was within 30 nm from the plasma membrane. Data are presented as mean ± SEM. The position of mGluR1b and mGluR5 immunogold particles distributed in the thorny excrescences relative to the postsynaptic specializations was also measured. 211 (114 with mGluR1b and 97 with mGluR5) out of the 247 thorny excrescences showing prominent postsynaptic specializations in the electron microscope were considered in this analysis. Digitized electron micrographs of the thorny excrescences were taken at 28,000x and the frequency of immunoparticles was measured in 60 nm–wide segments taken from the edge of the postsynaptic density. Since three samples analyzed did not differ in particle distribution (Kolmogorov Smirnov test, $P > 0.19$), the data were pooled. Image–J was used to measure gold particle's distance counted from the edge of the postsynaptic specialization, and the values were analyzed and displayed using GraphPad Prism 4.

Supplementary Material

Refer to Web version on PubMed Central for supplementary material.

Acknowledgments

We would like to thank members of the Castillo lab (in particular Andrés Chávez, Thomas Younts, Paola Haeger and Sachin Makani) for their constructive discussions on the data and helpful comments on the manuscript. This work was supported by NIH grants to P.E.C. (R01 MH081935 and R01 DA017392). Funding for P.G.'s laboratory is provided by MICINN (SAF2009–07065), Basque Country Government (GIC07/70–IT–432–07) and University of the Basque Country UPV/EHU (UFI11/41)..

REFERENCES

1. Daw NW, Stein PS, Fox K. The role of NMDA receptors in information processing. Annu Rev Neurosci. 1993; 16:207–222. [PubMed: 8460891]
2. Hunt DL, Castillo PE. Synaptic plasticity of NMDA receptors: mechanisms and functional implications. Current Opinion in Neurobiology. 2012 (in press).
3. Traynelis SF, et al. Glutamate receptor ion channels: structure, regulation, and function. Pharmacol Rev. 2010; 62:405–496. [PubMed: 20716669]
4. Schiller J, Schiller Y. NMDA receptor-mediated dendritic spikes and coincident signal amplification. Curr Opin Neurobiol. 2001; 11:343–348. [PubMed: 11399433]
5. Herron CE, Lester RA, Coan EJ, Collingridge GL. Frequency-dependent involvement of NMDA receptors in the hippocampus: a novel synaptic mechanism. Nature. 1986; 322:265–268. [PubMed: 2874493]
6. Kwon HB, Castillo PE. Long-term potentiation selectively expressed by NMDA receptors at hippocampal mossy fiber synapses. Neuron. 2008; 57:108–120. [PubMed: 18184568]
7. Rebola N, Lujan R, Cunha RA, Mulle C. Adenosine A2A receptors are essential for long-term potentiation of NMDA-EPSCs at hippocampal mossy fiber synapses. Neuron. 2008; 57:121–134. [PubMed: 18184569]
8. Nicoll RA, Schmitz D. Synaptic plasticity at hippocampal mossy fibre synapses. Nat Rev Neurosci. 2005; 6:863–876. [PubMed: 16261180]
9. Jonas P, Major G, Sakmann B. Quantal components of unitary EPSCs at the mossy fibre synapse on CA3 pyramidal cells of rat hippocampus. J Physiol. 1993; 472:615–663. [PubMed: 7908327]
10. Rebola N, Carta M, Lanore F, Blanchet C, Mulle C. NMDA receptor-dependent metaplasticity at hippocampal mossy fiber synapses. Nat Neurosci. 2011; 14:691–693. [PubMed: 21532578]
11. Astori S, Pawlak V, Kohr G. Spike-timing-dependent plasticity in hippocampal CA3 neurons. J Physiol. 2010; 588:4475–4488. [PubMed: 20876200]
12. Henze DA, Wittner L, Buzsaki G. Single granule cells reliably discharge targets in the hippocampal CA3 network in vivo. Nat Neurosci. 2002; 5:790–795. [PubMed: 12118256]
13. Marr D. Simple memory: a theory for archicortex. Philos Trans R Soc Lond B Biol Sci. 1971; 262:23–81. [PubMed: 4399412]
14. Jung MW, McNaughton BL. Spatial selectivity of unit activity in the hippocampal granular layer. Hippocampus. 1993; 3:165–182. [PubMed: 8353604]
15. Caporale N, Dan Y. Spike timing-dependent plasticity: a Hebbian learning rule. Annu Rev Neurosci. 2008; 31:25–46. [PubMed: 18275283]
16. Lujan R, Nusser Z, Roberts JD, Shigemoto R, Somogyi P. Perisynaptic location of metabotropic glutamate receptors mGluR1 and mGluR5 on dendrites and dendritic spines in the rat hippocampus. Eur J Neurosci. 1996; 8:1488–1500. [PubMed: 8758956]
17. Morishita W, Marie H, Malenka RC. Distinct triggering and expression mechanisms underlie LTD of AMPA and NMDA synaptic responses. Nat Neurosci. 2005; 8:1043–1050. [PubMed: 16025109]
18. Peng Y, et al. Distinct trafficking and expression mechanisms underlie LTP and LTD of NMDA receptor-mediated synaptic responses. Hippocampus. 2010; 20:646–658. [PubMed: 19489005]

19. Ireland DR, Abraham WC. Mechanisms of group I mGluR-dependent long-term depression of NMDA receptor-mediated transmission at Schaffer collateral-CA1 synapses. J Neurophysiol. 2009; 101:1375–1385. [PubMed: 19109458]
20. Abraham WC. Metaplasticity: tuning synapses and networks for plasticity. Nat Rev Neurosci. 2008; 9:387–399. [PubMed: 18401345]
21. Kobayashi K, Poo MM. Spike train timing-dependent associative modification of hippocampal CA3 recurrent synapses by mossy fibers. Neuron. 2004; 41:445–454. [PubMed: 14766182]
22. Kapur A, Yeckel M, Johnston D. Hippocampal mossy fiber activity evokes Ca2+ release in CA3 pyramidal neurons via a metabotropic glutamate receptor pathway. Neuroscience. 2001; 107:59–69. [PubMed: 11744247]
23. Ross WN. Understanding calcium waves and sparks in central neurons. Nat Rev Neurosci. 2012; 13:157–168. [PubMed: 22314443]
24. Nakashiba T, Buhl DL, McHugh TJ, Tonegawa S. Hippocampal CA3 output is crucial for ripple-associated reactivation and consolidation of memory. Neuron. 2009; 62:781–787. [PubMed: 19555647]
25. Nakazawa K, et al. Requirement for hippocampal CA3 NMDA receptors in associative memory recall. Science. 2002; 297:211–218. [PubMed: 12040087]
26. Nakazawa K, et al. Hippocampal CA3 NMDA receptors are crucial for memory acquisition of one-time experience. Neuron. 2003; 38:305–315. [PubMed: 12718863]
27. Leutgeb S, Leutgeb JK, Moser MB, Moser EI. Place cells, spatial maps and the population code for memory. Curr Opin Neurobiol. 2005; 15:738–746. [PubMed: 16263261]
28. Torborg CL, Nakashiba T, Tonegawa S, McBain CJ. Control of CA3 output by feedforward inhibition despite developmental changes in the excitation-inhibition balance. J Neurosci. 2010; 30:15628–15637. [PubMed: 21084618]
29. Mori M, Abegg MH, Gahwiler BH, Gerber U. A frequency-dependent switch from inhibition to excitation in a hippocampal unitary circuit. Nature. 2004; 431:453–456. [PubMed: 15386013]
30. Kumar A, Rotter S, Aertsen A. Spiking activity propagation in neuronal networks: reconciling different perspectives on neural coding. Nat Rev Neurosci. 2010; 11:615–627. [PubMed: 20725095]
31. Lisman JE. Bursts as a unit of neural information: making unreliable synapses reliable. Trends Neurosci. 1997; 20:38–43. [PubMed: 9004418]
32. Harnett MT, Bernier BE, Ahn KC, Morikawa H. Burst-timing-dependent plasticity of NMDA receptor-mediated transmission in midbrain dopamine neurons. Neuron. 2009; 62:826–838. [PubMed: 19555651]
33. Sjostrom PJ, Nelson SB. Spike timing, calcium signals and synaptic plasticity. Curr Opin Neurobiol. 2002; 12:305–314. [PubMed: 12049938]
34. Lisman J. A mechanism for the Hebb and the anti-Hebb processes underlying learning and memory. Proc Natl Acad Sci U S A. 1989; 86:9574–9578. [PubMed: 2556718]
35. Valenti O, Conn PJ, Marino MJ. Distinct physiological roles of the Gq-coupled metabotropic glutamate receptors Co-expressed in the same neuronal populations. J Cell Physiol. 2002; 191:125–137. [PubMed: 12064455]
36. Topolnik L, Azzi M, Morin F, Kougioumoutzakis A, Lacaille JC. mGluR1/5 subtype-specific calcium signalling and induction of long-term potentiation in rat hippocampal oriens/alveus interneurones. J Physiol. 2006; 575:115–131. [PubMed: 16740609]
37. Gerber U, Gee CE, Benquet P. Metabotropic glutamate receptors: intracellular signaling pathways. Curr Opin Pharmacol. 2007; 7:56–61. [PubMed: 17055336]
38. Frausto SF, Ito K, Marszalec W, Swanson GT. A novel form of low-frequency hippocampal mossy fiber plasticity induced by bimodal mGlu1 receptor signaling. J Neurosci. 2011; 31:16897–16906. [PubMed: 22114260]
39. Wang HX, Gerkin RC, Nauen DW, Bi GQ. Coactivation and timing-dependent integration of synaptic potentiation and depression. Nat Neurosci. 2005; 8:187–193. [PubMed: 15657596]
40. Buzsaki G. Neural syntax: cell assemblies, synapsembles, and readers. Neuron. 2010; 68:362–385. [PubMed: 21040841]

41. Bains JS, Longacher JM, Staley KJ. Reciprocal interactions between CA3 network activity and strength of recurrent collateral synapses. Nat Neurosci. 1999; 2:720–726. [PubMed: 10412061]
42. Lawrence JJ, McBain CJ. Interneuron diversity series: containing the detonation--feedforward inhibition in the CA3 hippocampus. Trends Neurosci. 2003; 26:631–640. [PubMed: 14585604]
43. Pouille F, Scanziani M. Enforcement of temporal fidelity in pyramidal cells by somatic feed-forward inhibition. Science. 2001; 293:1159–1163. [PubMed: 11498596]
44. Debanne D, Gahwiler BH, Thompson SM. Long-term synaptic plasticity between pairs of individual CA3 pyramidal cells in rat hippocampal slice cultures. J Physiol. 1998; 507(Pt 1):237–247. [PubMed: 9490845]
45. Song S, Miller KD, Abbott LF. Competitive Hebbian learning through spike-timing-dependent synaptic plasticity. Nat Neurosci. 2000; 3:919–926. [PubMed: 10966623]
46. Tsukamoto M, et al. Mossy fibre synaptic NMDA receptors trigger non-Hebbian long-term potentiation at entorhino-CA3 synapses in the rat. J Physiol. 2003; 546:665–675. [PubMed: 12562995]
47. Major G, Polsky A, Denk W, Schiller J, Tank DW. Spatiotemporally graded NMDA spike/plateau potentials in basal dendrites of neocortical pyramidal neurons. J Neurophysiol. 2008; 99:2584–2601. [PubMed: 18337370]
48. Branco T, Hausser M. Synaptic integration gradients in single cortical pyramidal cell dendrites. Neuron. 2011; 69:885–892. [PubMed: 21382549]
49. Nishiyama M, Hong K, Mikoshiba K, Poo MM, Kato K. Calcium stores regulate the polarity and input specificity of synaptic modification. Nature. 2000; 408:584–588. [PubMed: 11117745]
50. Hulme SR, Jones OD, Ireland DR, Abraham WC. Calcium-Dependent But Action Potential-Independent BCM-Like Metaplasticity in the Hippocampus. J Neurosci. 2012; 32:6785–6794. [PubMed: 22593048]
51. Mateos JM, et al. Immunocytochemical localization of the mGluR1b metabotropic glutamate receptor in the rat hypothalamus. J Comp Neurol. 1998; 390:225–233. [PubMed: 9453666]
52. Ferraguti F, et al. Immunohistochemical localization of the mGluR1beta metabotropic glutamate receptor in the adult rodent forebrain: evidence for a differential distribution of mGluR1 splice variants. J Comp Neurol. 1998; 400:391–407. [PubMed: 9779943]
53. Uchigashima M, et al. Subcellular arrangement of molecules for 2-arachidonoyl-glycerol-mediated retrograde signaling and its physiological contribution to synaptic modulation in the striatum. J Neurosci. 2007; 27:3663–3676. [PubMed: 17409230]
54. Tanaka J, et al. Gq protein alpha subunits Galphaq and Galpha11 are localized at postsynaptic extra-junctional membrane of cerebellar Purkinje cells and hippocampal pyramidal cells. Eur J Neurosci. 2000; 12:781–792. [PubMed: 10762307]

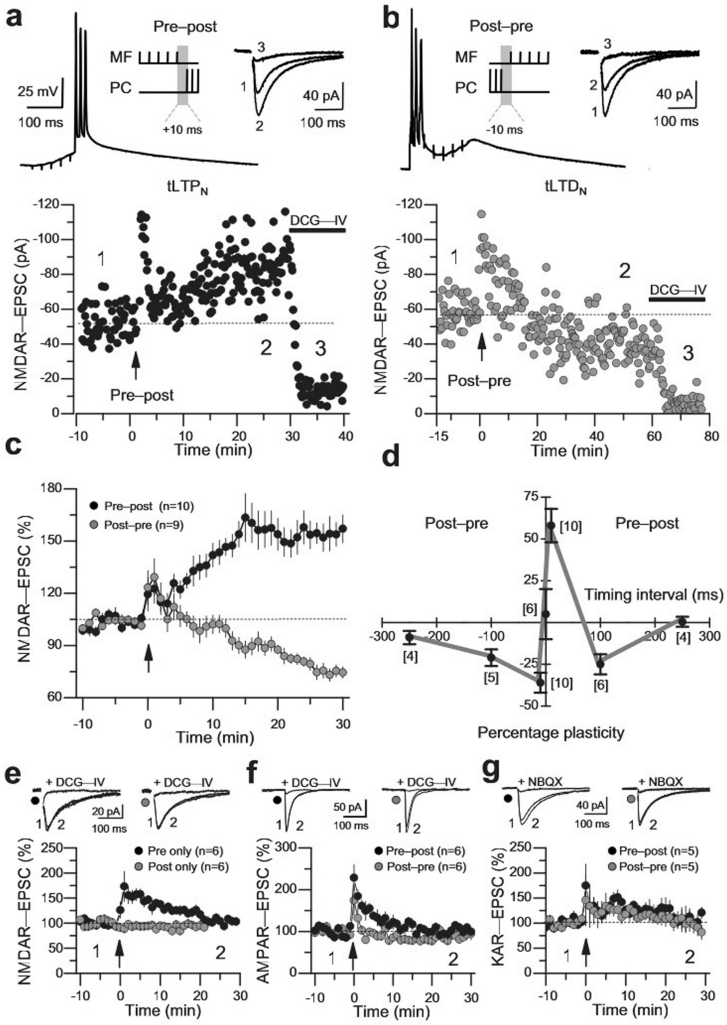

Figure 1. Bidirectional burst timing–dependent NMDAR plasticity

a,b) (*top*) Schematic of the induction protocol and example trace of a single pairing from the pre–post protocol. (*bottom*) Representative experiment for $tLTP_N$ induced by the pre–post protocol (100 pairings) at a time point indicated by the vertical arrow. Numbers indicate time points where averaged traces were taken (*top right*). The mGluR2/3 agonist DCG–IV (1 μM), which selectively abolishes MF synaptic transmission, was added to the perfusion at the end of all experiments. MF, mossy fiber; PC, CA3 pyramidal cell. **b**) Same as in a) except that a post–pre protocol (100 pairings) was used (*top*) and $tLTD_N$ was induced (*bottom*). **c**) Summary data (% plasticity) for $tLTP_N$ and $tLTD_N$. **d**) Learning rule generated by varying the timing interval of MF and PC bursts. Number of experiments for each timing inter–burst interval is indicated between brackets. **e**) Summary data for pre only (black circles; 103.1 ± 1.8% of baseline, n = 6; p = 0.2) and post only (grey circles; 91.8 ± 7.4% of baseline, n = 6; p = 0.3). **f**) Summary data for the effect of burst–timing induction protocols on MF–CA3 AMPAR–mediated transmission. No significant change was observed relative to baseline for the pre–post (p = 0.52) or post–pre (p = 0.33) induction protocols. **g**) Summary data for the effect of burst–timing induction protocols on MF–CA3 KAR–

mediated transmission. No significant change was observed relative to baseline for the pre–post ($p = 0.8$) or post–pre ($p = 0.21$) induction protocols. e–g, representative averaged traces are shown above. In all graphs, values represent mean ± s.e.m.

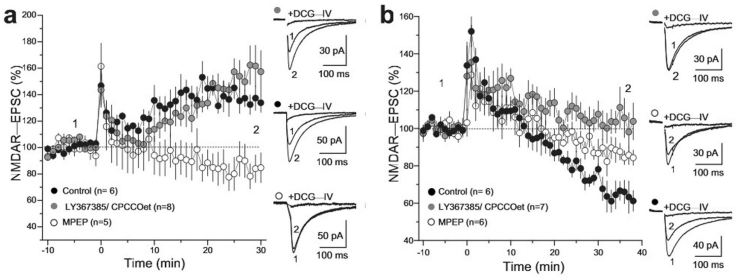

Figure 2. $tLTP_N$ and $tLTD_N$ exhibit differential sensitivity to Group–I mGluR antagonism

a) Pre–post $tLTP_N$ induction delivered in the continuous presence of the mGluR5 antagonist MPEP (4 μM) (white circles; 84.7 ± 10.4% of baseline, n = 6; p = 0.07) or the mGluR1 antagonists LY367385 (50 μM) or CPCCOet (50 μM) (grey circles; 152 ± 12% of baseline, n = 8, p = 0.0087). Compared to interleaved controls (black circles, 138 ± 5.7% of baseline, n = 6), $tLTP_N$ in MPEP was abolished (p = 0.0013), whereas in the presence of mGluR1 antagonists was normal (p = 0.2). **b**) Post–pre induction delivered in the presence of LY367385/CPCCOet (grey circles; 103.8 ± 4.8% of baseline, n = 7; p = 0.7) or MPEP (white circles; 84.4 ± 4.1% of baseline, n = 6; p = 0.0022). Compared to interleaved controls (black circles, 64.1 ± 9.0 % of baseline, n = 6), $tLTD_N$ was abolished in the presence of mGluR1 antagonists (p = 0.008), whereas it was partially sensitive to mGluR5 blockade (p = 0.029). Magnitude of plasticity was assessed 30–40 min post–tetanus. In both panels (a and b), representative averaged traces under each experimental condition are shown right. Values represent mean ± s.e.m.

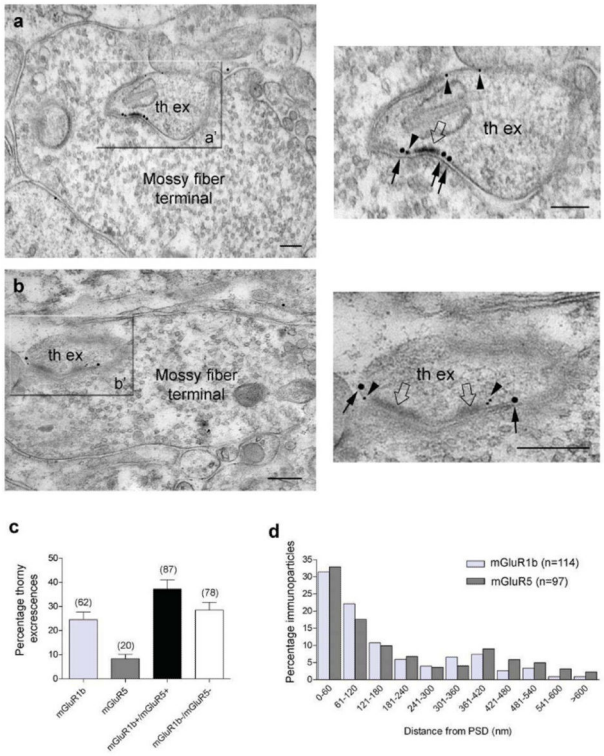

Figure 3. Immuno–electron microscopy of mGluR1b and mGluR5 at thorny excrescences

(**a**, **b**) Large MF synaptic terminals containing abundant round and clear synaptic vesicles make asymmetric synapses with thorny excrescences (th ex) emerging from the proximal apical dendrites of CA3 pyramidal neurons. MF synapses (framed areas **a'** and **b'**) have mGluR1b (small 10 nm–gold particles, arrowheads) and mGluR5 (large 20 nm–gold particles, arrows) in dendritic thorny membranes away from the postsynaptic density (hollow arrows). Scale bars: 0.5 μm. **c**) Percentages (mean ± S.E.M.) of thorny excrescences (n = 247) containing mGluR1b (24.5 ± 3.2%), mGluR5 (8.3 ± 1.9%), both mGluR1b + mGluR5 (37.2 ± 3.8%) or no mGluR1b–mGluR5 (28.5 ± 3.2%). **d**) Distribution of mGluR1b and mGluR5 immunolabeling in thorny excrescences of CA3 pyramidal neurons. Thorny membranes were divided into 60–nm–wide bins starting from the edge of the postsynaptic density. Data are expressed as frequency distribution (across the 60 nm segments) normalized to the total number of particles. Columns display the proportion of immunogold particles for each bin. Both receptor subtypes show a preferential perisynaptic distribution, i.e., within 60 nm from the edge of the postsynaptic specialization. About 32% of mGluR1b and ≈33% of mGluR5 are located in the perisynaptic zone.

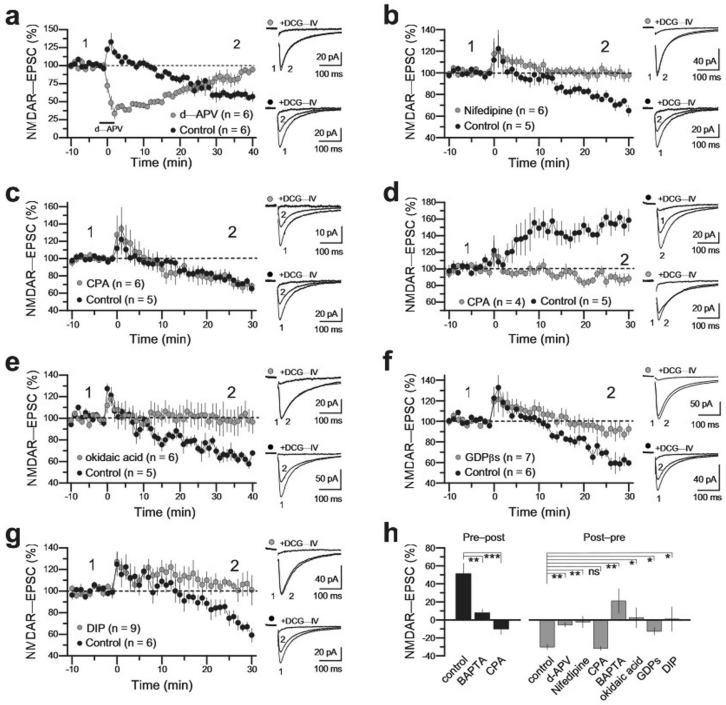

Figure 4. Mechanistic properties of $tLTP_N$ and $tLTD_N$

a) $tLTD_N$ requires NMDAR activation. Transient application of d–APV (25 μM) prior to induction blocked $tLTD_N$. In all panels, representative averaged traces under each experimental condition are shown right. **b**) $tLTD_N$ requires Ca^{2+} influx through L–type calcium channels. Delivering the POST–PRE induction in the presence of 10 μM nifedipine abolished $tLTD_N$ **c**) Pre–treatment (30 min prior to induction) and bath application of 30 μM cyclopiazonic acid (CPA) had no effect on $tLTD_N$ relative to interleaved controls. **d**) Depletion of intracellular Ca^{2+} stores by CPA abolished $tLTP_N$, demonstrating the unique additional requirement of store Ca^{2+} for $tLTP_N$. Interleaved control experiments are shown in black. **e**) $tLTD_N$ is blocked in the presence of 1 μM okadaic acid implicating phosphatase activity in the expression of $tLTD_N$. **f)** Intracellular loading of 600 μM GDPβS abolishes $tLTD_N$ indicating that a GTP dependent process is required for $tLTD_N$**. g**) $tLTD_N$ is blocked by intracellular loading of dynamin inhibitory peptide (DIP, 50 μM) implicating dynamin dependent endocytosis in the expression of $tLTD_N$. **h**) Summary data for all experimental groups representing the mean ± s.e.m. *p < 0.05; **p<0.01; ***p<0.001; n.s., not significant.

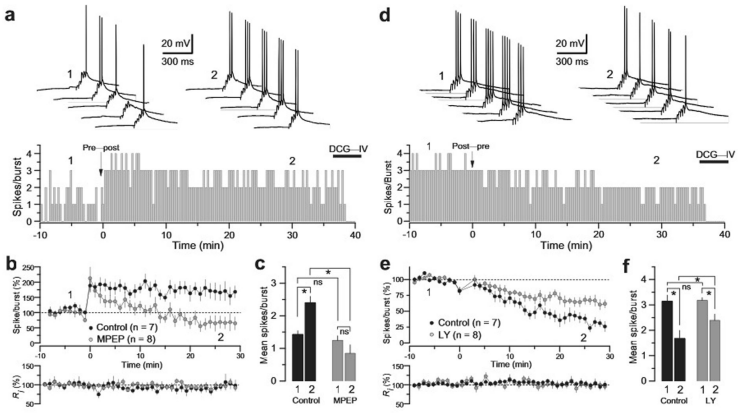

Figure 5. Plasticity of mossy fiber–driven burst–firing output endowed by $tLTP_N$ and $tLTD_N$

a) Representative single experiment of burst plasticity induced by the PRE–POST protocol (100 pairings, no drugs present in the bath). Number of spikes per burst are plotted against time. Sample traces from times indicated are shown above. **b**) Summary data of control and MPEP block experiments with accompanying input resistances. **c**) Quantification of the absolute value of mean spike counts pre (control: 1.4 ± 0.12 spikes, n = 7; MPEP: 1.2 ± 0.15 spikes, n = 8; p = 0.4, unpaired t–test) and post–tetanus (control: 2.4 ± 0.19 spikes; MPEP: 1.1 ± 0.18 spikes; p = 0.0092, unpaired t–test) for experiments shown in (b). **d**) Representative single experiment of POST–PRE (100 pairings) induced burst plasticity. **e**) Summary data for control including LY367385 block experiments with associated input resistances. **f**) Quantification of mean spikes/burst pre (control: 3.1 ± 0.25 spikes, n = 7; LY367385: 3.0 ± 0.16 spikes, n = 7; p = 0.37, unpaired t–test) and post–tetanus (control: 1.6 ± 0.4 spikes; LY367385: 2.3 ± 0.25 spikes; p = 0.037, unpaired t–test). Summary data represent mean ± s.e.m. *p < 0.05; n.s., not significant.

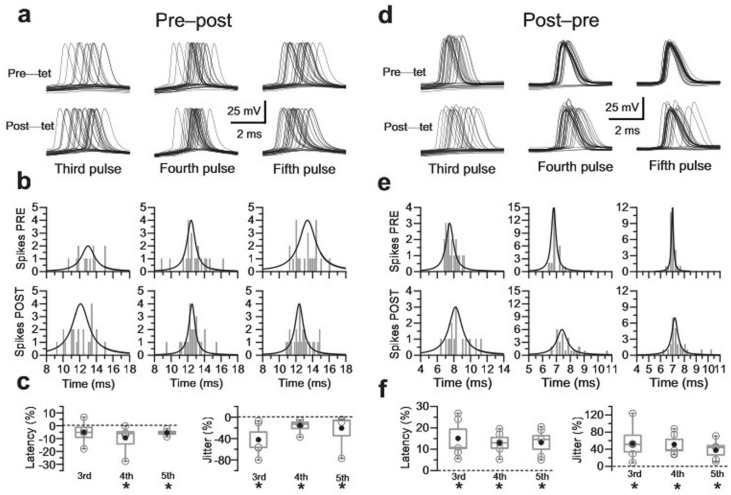

Figure 6. Bidirectional modulation of CA3 spike temporal fidelity

a) Representative superimposed traces taken from 30 consecutive sweeps of a single whole cell recording before (Pre–tet), and after (Post–tet) the pre–post induction protocol. **b**) Spike count histograms (from traces in a) of latency values fitted with a Lorentz curve. Peak offset represents the shift in latency from the stimulation pulse, and curve width the change in jitter. **c**) Box chart summarizing data from 5 cells. Both latency and jitter are represented as percent change relative to the pre–tetanus condition. **d**) Same as in (a) except the post–pre induction protocol was delivered. **e**) Same as in (b) except for $tLTD_N$. **f**) Same as in (c) for 5 $tLTD_N$ cells. Summary data represent mean ± s.e.m. *$p < 0.05$; n.s., not significant.

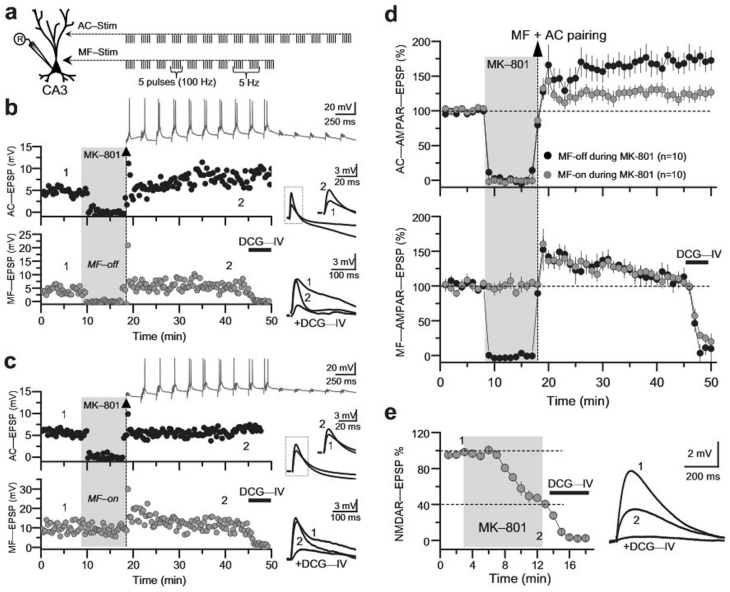

Figure 7. Heterosynaptic plasticity mediated by MF–NMDARs

a) Schematic of recording configuration and stimulation paradigm. **b**) (*Left*) Representative experiment where both AC–NMDARs and MF–NMDARs (*MF–off*) were protected from MK–801 blockade by stopping stimulation during MK–801 wash–in (shadow area). Synaptic responses were elicited by MF or AC single stimulations and recorded in current–clamp mode. Vertical arrow indicates time at which MF + AC paring was delivered (tetanus trace is shown above). (*Right*) Sample traces (averages of 20 individual responses) from time points indicated on the left. Extended time scale is shown for AC–peak EPSP indicated by a square box (*inset*). **c**) Same as in (b) for the condition where MF–NMDARs were selectively blocked by stimulating during MK–801 wash–in (*MF–on*). **d**) Superimposed summary data for both conditions illustrating the attenuation of AC–LTP when MF–NMDARs were partially blocked during induction (*Top*, *MF–on* 127 ± 9 % of baseline vs. *MF–off* 173 ± 17 % of baseline; p = 0.0017, unpaired t–test). No change in MF–AMPAR–EPSP amplitude was observed 30 min post tetanus (*Bottom*, *MF–on* 102 ± 6 % of baseline vs. *MF–off* 101 ± 8 % of baseline, p = 0.3, unpaired t–test). **e**) Isolated NMDAR–EPSPs demonstrating the degree of MK–801 blockade achieved during the 10 min MK–801 wash–in period (40 ± 4 % of baseline, n = 5, p = 0.0055, paired t–test). Representative traces are shown on the *right*. Summary data represent mean ± s.e.m.

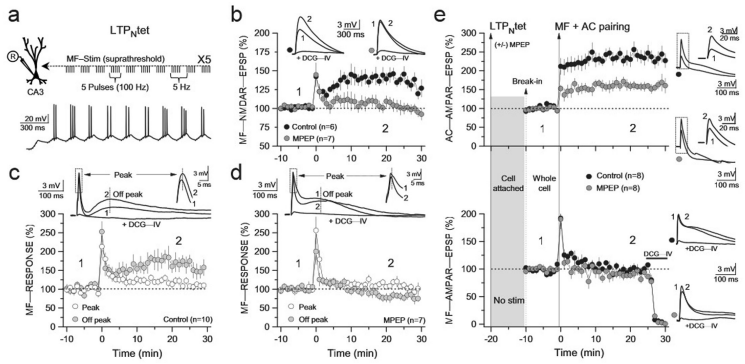

Figure 8. Heterosynaptic metaplasticity mediated by NMDAR LTP

a) (*Top*) schematic of experimental design and structure of LTP_N induction tetanus (LTP_Ntet) (*Bottom*) Example trace of suprathreshold MF burst stimulation used to elicit potentiation of MF–CA3 NMDAR transmission (LTP_N). **b**) LTP_Ntet potentiates MF NMDAR–EPSPs. NMDAR–EPSPs were recorded in the presence of NBQX (10 μM), picrotoxin (100 μM) and CGP 55845 (3 μM). (*Bottom*) Control LTP_N summary data (black circles 134 ± 8 % of baseline, n = 6; p = 0.0041) with interleaved MPEP (4 μM) block experiments (grey circles, 99 ± 4 % of baseline, n = 7; p = 0.4). Representative traces from time points indicated for either condition are shown above. **c**) LTP_Ntet selectively potentiates the Off–peak component of mixed MF–responses. Example traces of mixed MF–responses (*top*), dashed lines indicate where Peak and Off–peak measurements were taken [Peak 111 ± 8 % of baseline (p = 0.09) vs Off–peak 158 ± 12 % of baseline (p = 0.002), n = 10]. Traces indicate pre tetanus (1) and post tetanus (2) time points. Summary data is shown below highlighting the selective potentiation of the slow component of the mixed MF–response. **d**) Same as in (c) except 4 μM MPEP was used to block Off–peak potentiation [Peak 109 ± 11% baseline, n = 7; p = 0.17 vs. control PEAK responses (unpaired t– test). Off–peak 78 ± 8 % baseline, n =7; p = 0.0029 vs. control Off–peak responses (unpaired t–test). **e**) Two–pathway experiment (MF + AC pathways) designed to test the role of LTP_N in heterosynaptic metaplasticity. The LTP_N–inducing tetanus was delivered in the cell–attached recording configuration (t = –20 min) in the presence (+) or absence (–) of 4 μM MPEP. Following a 10 min period devoid of stimulation (shaded area), whole–cell recording configuration was obtained (break–in, t = –10 min) and a 10 min baseline was acquired. At t = 0, when LTP_N is robust (i.e. 20 min post–tetanus) the MF + AC pairing induction (as illustrated in Fig. 7a) was delivered to elicit heterosynaptic plasticity. (*top*) When LTP_N is blocked by MPEP (grey circles), AC–LTP is attenuated compared to the control (black circles) (control; 158 ± 7 % of baseline, n = 8, *vs*. MPEP; 234 ± 22 % of baseline, n = 8; p = 0.0038, non–paired t–test), while the MF–AMPAR–EPSP is unaffected in either case (*bottom*). Representative traces of both pathways, for each condition (+/–) MPEP are shown on right. Summary data represent mean ± s.e.m.; ns, not significant.